Polymer 332 (2025) 128575

Contents lists available at ScienceDirect

Polymer

journal homepage: www.elsevier.com/locate/polymer

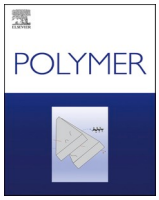

Strain-induced crystallization behaviors of natural rubber with additional lipids

Tomoaki Nakatsuka [a], Hiroyasu Masunaga [b], Yui Tsuji [a], Keiji Numata [a,c,d,*]

[a] Department of Material Chemistry, Graduate School of Engineering, Kyoto University, Kyoto Daigaku Katsura, Nishikyo-ku, Kyoto, 615-8510, Japan
[b] Japan Synchrotron Radiation Research Institute, Sayo-gun, Hyogo, 679-5198, Japan
[c] Biomacromolecules Research Team, RIKEN Center for Sustainable Resource Science, 2-1 Hirosawa, Wako, Saitama, 351-0198, Japan
[d] Institute for Advanced Biosciences, Keio University, Nipponkoku 403-1, Daihouji, Tsuruoka, Yamagata, 997-0017, Japan

ARTICLE INFO

Keywords:
Natural rubber
Strain-induced crystallization (SIC)
Differential scanning calorimeter (DSC)
Wide-angle X-ray diffraction (WAXD)
Nucleating agent effect
Naturally occurring network

ABSTRACT

Natural rubber (NR) is an indispensable material in our daily lives due to its excellent properties derived from strain-induced crystallization (SIC). However, the mechanism and the promoting factor of SIC have not been clarified yet, and the influence of non-rubber components to SIC has long been discussed. This study aims to elucidate the mechanisms through which non-rubber components enhance SIC, by mixing NR with three different lipids—glycerol monostearate (GMS), glycerol distearate (GDS), and glycerol tristearate (GTS)—and examining their effects on SIC behavior and tensile properties. The results revealed that GTS microcrystals act as nucleating agents within the NR matrix, lowering the energy required for SIC nucleation, and promote the SIC onset, even though the SIC promotion did not affect significantly on the tensile properties. This nucleating effect of GTS is attributed to the combination of the strong affinity with NR ensured by high hydrophobicity and its highly crystalline due to efficient packing of its alkyl chains. In contrast, GMS and GDS, possessing hydroxyl groups, did not act as a nucleating agent, but rather delayed the SIC by lowering crosslink density. These findings suggest that the dominant SIC-promoting factor is nucleating effect in this solution mixing system, and hydroxyl groups of the lipids seems not to interact with the functional groups of NR chain ends to form end-linking structure. This perspective is expected to advance the understanding of SIC mechanisms and guide future research in this field.

1. Introduction

Natural rubber (NR) is widely used in various fields of our daily life, particularly in the tire industry, due to its superior properties such as good elasticity, high tensile strength and crack growth resistance. These outstanding properties are believed to arise from a phenomenon called strain-induced crystallization (SIC), which is caused by the alignment of polymer chains during stretching [1,2]. Generally, SIC in NR is known to occur at lower strains compared to synthetic *cis*-1,4-polyisoprene rubber (IR) [3,4]. However, the dominant factor and the detailed mechanisms of SIC remain unclear, and the SIC behavior of NR has not yet been fully replicated by IR or other polymeric materials.

NR is derived from the latex obtained from the rubber tree (*Hevea brasiliensis*), containing not only the main component, *cis*-1,4-polyisoprene, but also approximately 6 % non-rubber components such as proteins, lipids and fatty acids [5]. As the proposed factors promoting SIC in NR, high stereoregularity of *cis*-configuration and the presence of non-rubber components have long been considered essential for efficient SIC. However, even when the stereoregularity is modified to the same level of IR by introducing *trans*-configuration, NR still shows the superior mechanical properties [6], which has drawn significant attention to the role of non-rubber components as a determining factor of SIC behavior in NR. Thus, we still face the long-standing question: how do non-rubber components promote SIC behavior? There are two primary hypotheses for that question. The first hypothesis suggests that interactions between the terminal structures of NR molecules and non-rubber components form a network through physical crosslinking, called naturally occurring network, thereby increasing crosslink density and promoting SIC [7–9]. Recent advanced NMR analysis clarified that NR molecules have two types of terminal groups, an α-terminal, which

* Corresponding author. Department of Material Chemistry, Graduate School of Engineering, Kyoto University, Kyoto Daigaku Katsura, Nishikyo-ku, Kyoto, 615-8510, Japan.
E-mail address: keiji.numata@riken.jp (K. Numata).

https://doi.org/10.1016/j.polymer.2025.128575
Received 4 March 2025; Received in revised form 9 May 2025; Accepted 20 May 2025
Available online 20 May 2025

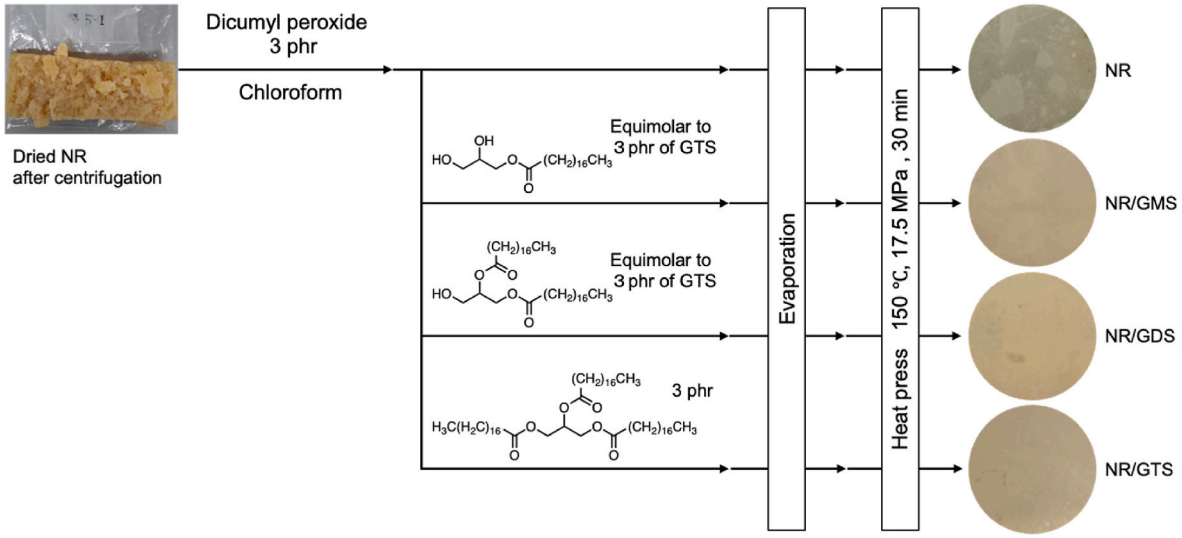

Fig. 1. The sample preparation process of NR, NR/GMS, NR/GDS, and NR/GTS.

has been identified as containing ester or hydroxyl groups, and an ω-terminal, which is connected to *trans*-oligoisoprene units [10–12]. Therefore, it is proposed that the hydroxyl groups of non-rubber components form hydrogen bonds with the hydroxyl groups at the α-terminal of NR chains, creating a crosslinked structure [13,14]. The second hypothesis suggests that non-rubber components act as nucleating agents during the SIC process. Some previous studies have suggested that fatty acids present in NR function as nucleating agents, helping crystal nucleation and growth of SIC [15,16].

Given these hypotheses, the current study aims to clarify the role of non-rubber components, particularly lipids, in influencing the SIC performance of NR. Here, we seek to determine whether these lipids contribute to the formation of a naturally occurring network or act as nucleating agents, by adding lipids in NR and characterizing the mechanical properties. As additional lipids, glycerol monostearate (GMS), glycerol distearate (GDS), and glycerol tristearate (GTS) were selected. They are the derivatives of glycerol and stearic acid, differentiated by the number of stearic acid molecules esterified to glycerol. They have varying numbers of hydroxyl groups and esterified fatty acids, while maintaining the complementary relationship in chemical structure. Stearic acid is abundantly present in natural rubber and has been reported to potentially promote the nucleation of SIC [15]. Therefore, these lipids were considered suitable for determining whether the dominant effect on SIC behavior arises from network formation via physical crosslinking derived from hydroxyl groups or the nucleating agent effect derived from esterified fatty acids. The current results demonstrated that the addition of GTS promoted the onset of SIC, while GMS and GDS delayed it, indicating that the nucleating agent effect plays a dominant role in the current system. Furthermore, a new insight was introduced to explain the relationship between strain and crystallinity, related to the thermal-induced crystallization of materials. From this perspective, the SIC behavior of pure NR can be described as "superstretching", analogous to supercooling of a liquid. This new insight will help to deepen the understanding of SIC behavior in NR.

2. Materials & methods/experimental procedure

2.1. Materials

The dried NR sample was provided by Bridgestone Corporation (Tokyo, Japan). The original latex was obtained from *Hevea brasilliensis* and centrifuged once to reduce the composition of non-rubber components. It was dried after acid coagulation. The nitrogen content was 0.17 % (w/w), the gel content was 4.67 % (w/w), and the number-average molecular weight was measured as $M_n = 25 \times 10^4$ g/mol by gel permeation chromatography (GPC). GMS, GDS, and GTS were purchased from FUJIFILM Wako Pure Chemical Co. (Osaka, Japan). Dicumyl peroxide was purchased from Sigma-Aldrich (St. Louis, MO, USA). Chloroform, used as solvent, was analytical grade. All reagents were used without further purification.

2.2. Sample preparation

The dried NR (12 g) was dissolved into chloroform (480 mL) and thoroughly stirred overnight. Then dicumyl peroxide (3 phr) was added into the solution, and it was divided into portions of 60 mL. One portion is for control sample with no additional lipid. 3 phr of GTS was added to another portion, and equimolar amounts of GMS and GDS were added to the other portions, respectively. After mixing them for a while, the solvent was removed by using evaporator and left under vacuum condition for 2 h. They were put in a hollow metal plate with a thickness of 1 mm, sanded between two flat metal plate, and heat pressed at 150 °C, 17.5 MPa, for 30 min. The crosslinking reaction is assumed to proceed during this heating process. The obtained NR sheets, each having a thickness of 1 mm, were named as NR, NR/GMS, NR/GDS, and NR/GTS depending on the additional lipids, respectively (Fig. 1).

2.3. DSC measurement

Differential scanning calorimetry (DSC) measurements were performed using DSC 8500 instrument (PerkinElmer, Waltham, MA). The heat flow was calibrated with high-purity indium. Each sample sheet was punched into disc shape with 5 mm diameter (ca. 5 mg), encapsulated in aluminum pan, and loaded into the DSC instrument with an identical empty pan used as the reference. The samples were heated from −100 °C to 150 °C at a heating rate of 10 °C/min in nitrogen atmosphere.

2.4. FT-IR analysis

The Fourier-transform infrared (FT-IR) spectra of each sample were recorded on an IRPrestige-21 FT-IR spectrophotometer (Shimadzu Corporation, Kyoto, Japan) with a MIRacle A single-reflection attenuated total reflectance (ATR) unit using a Ge prism. The spectra from 700 to 4000 cm^{-1} were accumulated at 4 cm^{-1} resolution using 64 scans.

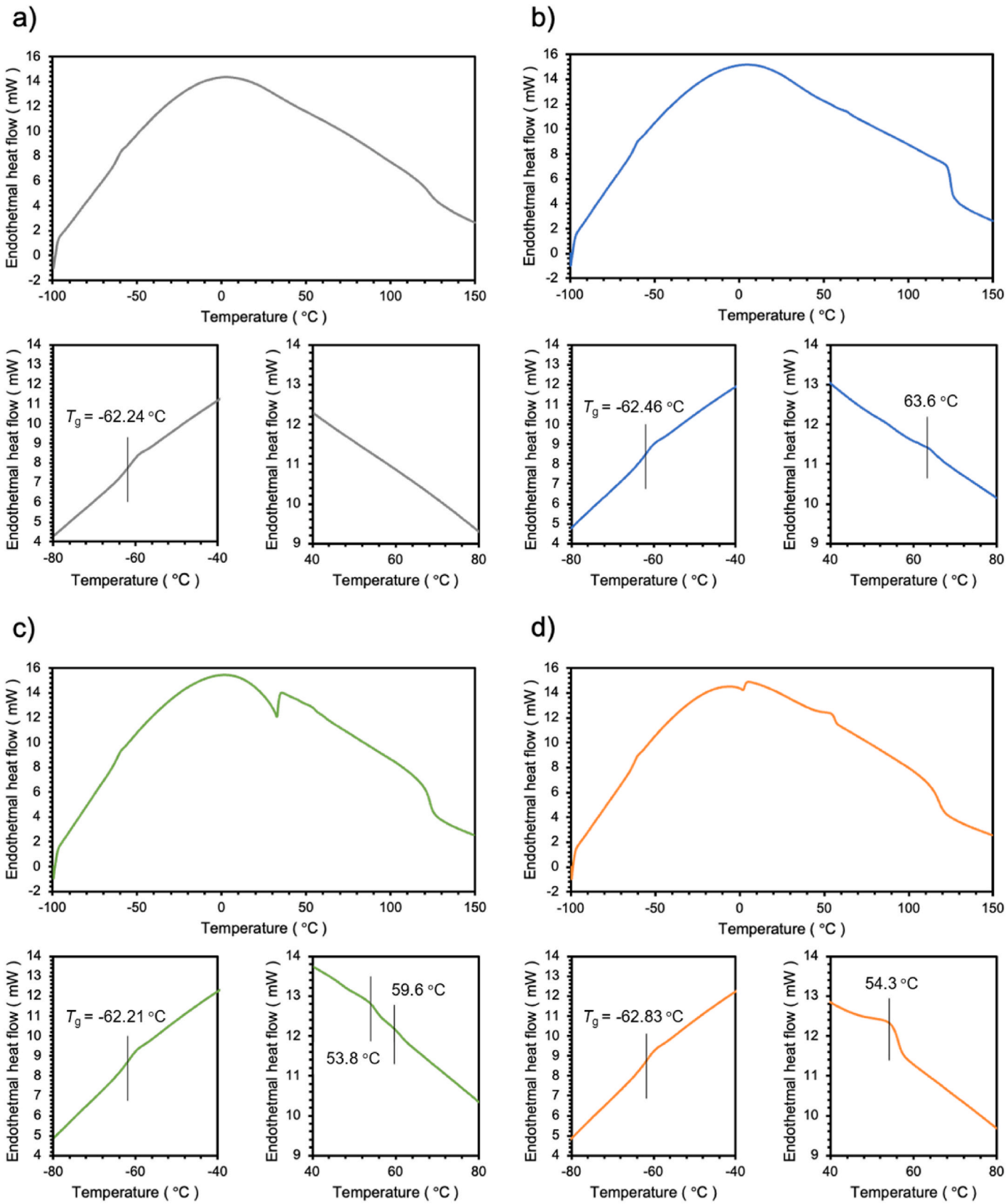

Fig. 2. The results of DSC analysis of a) NR, b) NR/GMS, c) NR/GDS, and d) NR/GTS to determine T_g and melting temperature of the additional lipids.

2.5. Swelling test

Swelling test was conducted in toluene. Each sample sheet was punched into disc shape with 5 mm diameter. They were immersed in toluene, and the mass of each sample was measured in every 10 min. After the mass stopped increasing, reaching the equilibrium, the swelling mass was measured, and the weight swelling rate was calculated using the value. The swelling ratio Q was calculated as follows,

$$Q = \frac{w_s - w_0}{w_0}$$

where w_0 is initial mass and w_s is equilibrium swelling mass. From the resulting value of Q, the crosslink density ν was calculated according to the following equations in the Flory-Rehner theory [17],

$$\nu = -\frac{ln(1-\phi_r) + \phi_r + \chi\phi_r^2}{V_0\left(\phi_r^{\frac{1}{3}} - \frac{\phi_r}{2}\right)}$$

$$\phi_r = \left(\frac{\rho_r}{\rho_s}Q + 1\right)^{-1}$$

where ϕ_r is the volume fraction of the polymer in the swollen network; V_0 is the molar volume of the solvent and χ is the Flory-Huggins polymer-solvent interaction parameter; ρ_s and ρ_r are the densities of the solvent and NR respectively. The following constant values were used to determine the crosslink density: $\rho_s = 0.867$ g/ml (toluene); $\rho_r = 0.930$ g/ml (NR); $V_0 = 106.3$ g/cm^3; $\chi = 0.39$ (NR-toluene) [18]. The measurement was conducted 3 times for each sample and average values were calculated.

2.6. Wide-Angle X-ray Diffraction (WAXD) measurement

The in-situ synchrotron WAXD measurements were conducted on BL05XU beamline in SPring-8 (Harima, Japan), using the X-ray wavelength of 1 Å. Each sample was punched into O-ring shape with 3 mm inner diameter and 5 mm outer diameter (Fig. S1). The ring-shaped samples were stretched between two moving pins under elongation rate of 20 mm/min and simultaneously X-rayed in interval of 1.5 s, which means WAXD images were obtained for each 0.5 mm stretch. The irradiation time was 1.0 s for all images. The obtained WAXD 2D images were converted to 1D profile by azimuthal integration using package Red2D (https://github.com/hurxl/Red2D) in Igor Pro 9.05 (WaveMetrics) and analyzed with multipeak fitting function to calculate crystallinity. The calculation of crystallinity was conducted using the WAXD patterns of one that onset strain of SIC was closest to the average value among the five trials. The crystallinity index χ_c was calculated according to the equation below.

$$\chi_c = \frac{A_{200} + A_{120}}{A_{\text{amorphous}} + A_{200} + A_{120}}$$

Here, A_{200}, A_{120}, and $A_{\text{amorphous}}$ are the area of divided peak assigned to (200) lattice, (120) lattice, and amorphous halo, respectively.

2.7. Tensile test

Tensile test was conducted with EZ-L instruments (Shimadzu, Kyoto, Japan) equipped with 50 N load cell. Each sample sheet was punched into O-ring shape with 8 mm inner diameter and 10 mm outer diameter (Fig. S2). The measurement was conducted 5 times for each sample. They were elongated at the rate of rate 300 %/min at room temperature to investigate tensile properties in the conditions of practical use such as pneumatic tires. The elastic modulus was obtained from the slope angle at 100 % strain and 400 % strain for each sample. They are used to measure as the parameter of the slow linier increase of stress before SIC and the progress of stress upturn that is often related to the SIC growth, respectively.

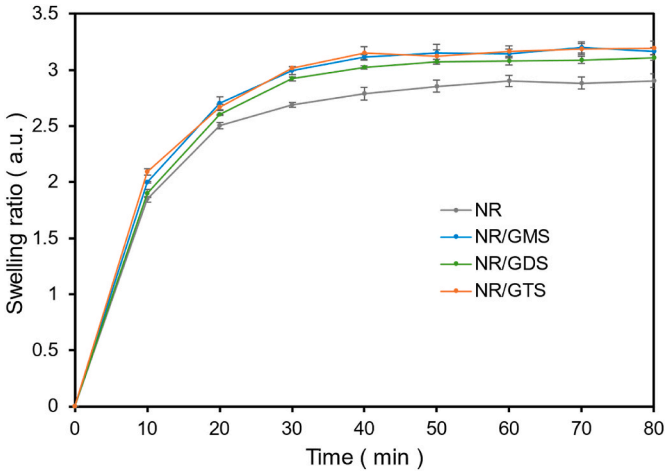

Fig. 3. The change of swelling ratio for NR, NR/GMS, NR/GDS and NR/GTS as a function of time.

3. Results and discussion

3.1. Miscibility of the additional lipids in NR

To investigate the miscibility and phase separation of NR and glycerol stearates, DSC measurement was conducted. Fig. 2 shows the resulting DSC curves for each sample. In this measurement, the glass transition temperature T_g was determined as the initial baseline step of the heat flow curve. The T_g of pure NR was calculated to be −62 °C (Fig. 2a), which was the same among all samples regardless of the addition of glycerol stearates. This value is in accordance with reported T_g of pure NR [19–21]. Furthermore, the endothermal peaks were observed at 63.6 °C for NR/GMS (Figs. 2b), 53.8 °C and 59.6 °C for NR/GDS (Figs. 2c), 54.3 °C for NR/GTS (Fig. 2d). These endothermic peaks correspond to the melting temperatures of additional glycerol stearates, respectively (Fig. S1). This result means that each glycerol stearate exists as a crystalline domain separated from the NR phase.

In addition, FI-IR analysis was conducted to investigate the molecular interaction between NR matrix and additional lipids. The characteristic peaks attributed to polyisoprene of NR chain were observed, however, peaks originating from the additional lipids were significantly smaller than those attributed to polyisoprene and could not be reliably evaluated. Although peaks corresponding to O–H or C═O groups present in the lipids, particularly the carbonyl peak around 1739 cm^{-1}, were detected, these functional groups were also present in NR itself, making it difficult to distinguish the contributions from the added lipids (Fig. S6).

3.2. Evaluation of the crosslink density

The change in swelling ratio against the immersion time is shown in Fig. 3, and resulting crosslink density of each sample is shown in Table 1. The results showed that the equilibrium swelling ratio became larger by adding lipids compared to pure NR, and the difference among GMS, GDS and GTS was negligible (Fig. 3). Accordingly, the addition of lipids resulted in the decrease of crosslink density, regardless of the lipid type (Table 1). Therefore, it is unlikely that the mixed lipids interact with the rubber molecules by forming hydrogen bond via hydroxyl groups or entanglement via alkyl chains. Considering the result in the previous section that glycerol stearates exist in NR matrix as crystal domain, it is reasonable to assume that the presence of lipid domains results in a decrease in crosslink density by occupying space without participating

Table 1
The crosslink density and parameters of NR NR/GMS, NR/GDS, and NR/GTS.

	Before swelling w_0 (mg)	After swelling w_s (mg)	Equilibrium swelling ratio Q (a.u.)	Crosslink density ν ($\times 10^{-4}$ mol/cm^3)
NR	15.44 ± 0.13	60.28 ± 0.99	2.90 ± 0.04	2.31 ± 0.06
NR/GMS	14.87 ± 0.03	61.98 ± 0.84	3.17 ± 0.06	1.97 ± 0.07
NR/GDS	15.38 ± 0.11	63.22 ± 0.86	3.11 ± 0.03	2.04 ± 0.03
NR/GTS	14.77 ± 0.04	61.99 ± 0.44	3.19 ± 0.03	1.94 ± 0.04

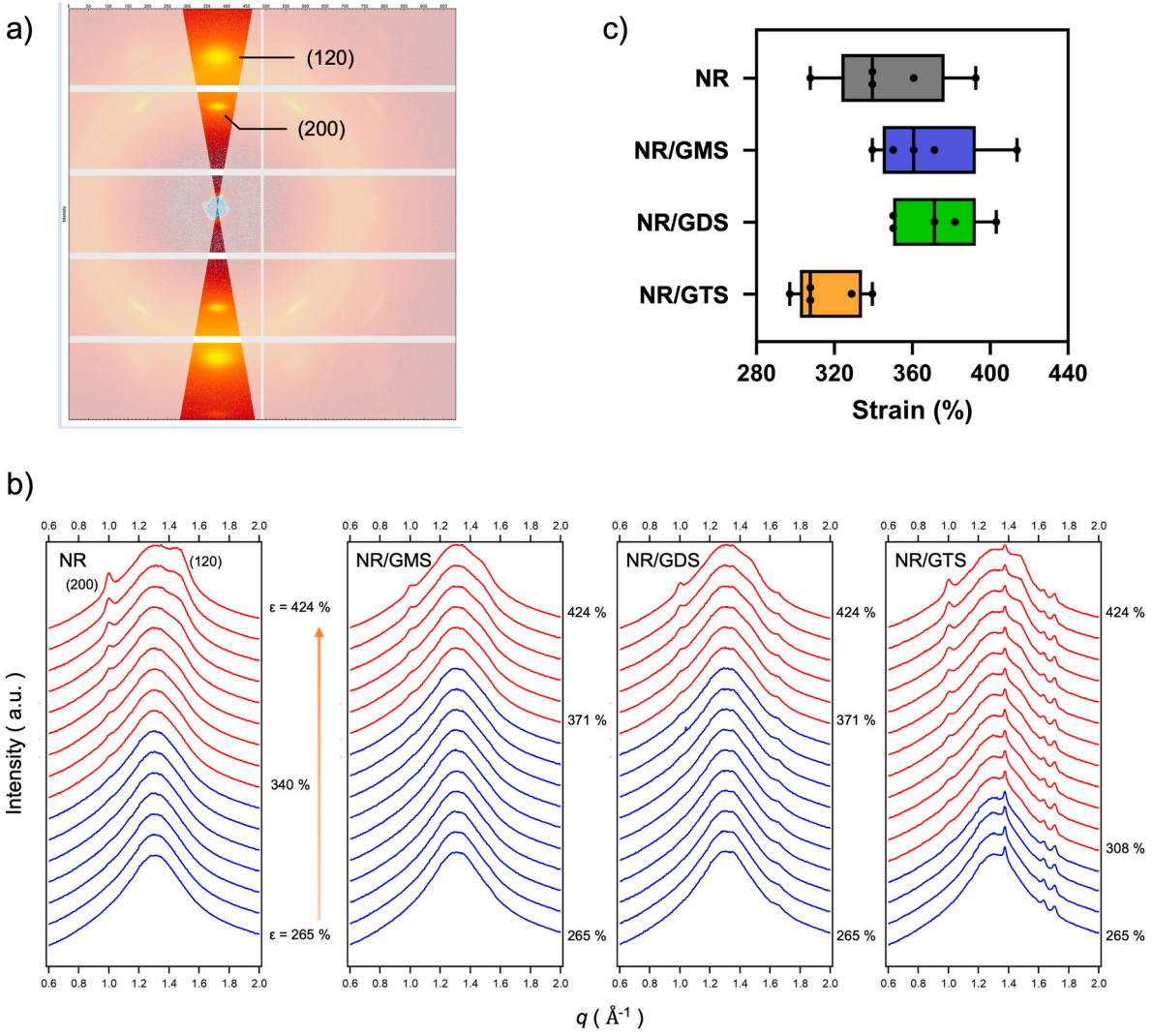

Fig. 4. a) 2D WAXD pattern of pure NR causing SIC. The integration for 1D pattern was carried out over the specified range in the picture. b) 1D WAXD patterns for NR, NR/GMS, NR/GDS, and GTS when it was stretched from 265 % to 424 % in strain. The displayed sample is the one whose SIC onset strain was closest to the average. The color change from blue to red with increase of strain indicate the SIC onset. c) Comparison of the onset strain of SIC. ($n = 5$). (For interpretation of the references to color in this figure legend, the reader is referred to the Web version of this article.)

in the crosslinking network.

3.3. SIC behavior

To observe the SIC behavior, the crystallization process during stretching was monitored using in-situ WAXD measurements. In this study, particular attention was paid to the onset strain of SIC for the evaluation of SIC performance. The collected 2D WAXD patterns were integrated azimuthally in the limited region ($\theta = 80°$–$100°$, Fig. 4a), and the 1D WAXD patterns were obtained for each sample (Fig. 4b). The onset strain of SIC was determined by the peak existence at $q = 1.00$ Å^{-1}, which is attributed to (200) lattice plane of NR crystal. For the pure NR in Fig. 4b, the broad amorphous halo, with its peak top at $q = 1.30$ Å^{-1}, was reserved during stretching, while the peak intensity at $q = 1.00$ Å^{-1} and $q = 1.48$ Å^{-1}, which is respectively attributed to (200) and (120) lattice plane, became larger as the strain increased. The (200) peak existed at the strain around 340 %, which was regarded as the onset strain of SIC. Compared to the peaks in NR profiles, the similar peaks were observed at higher strain in NR/GMS and NR/GDS, and lower strain in NR/GTS. Following this method, measurements were conducted five times for each sample, and the resulting data for the onset strain of SIC was summarized (Fig. 4c). This result suggests that the addition of GTS promoted the SIC onset compared to the pure NR, while GMS and GDS delayed the SIC onset. Furthermore, a weak peak at $q = 1.65$ was observed in NR/GDS, and clear peaks were found at $q = 1.38$, 1.63, and 1.71 in GTS. They are derived from the microcrystals of the

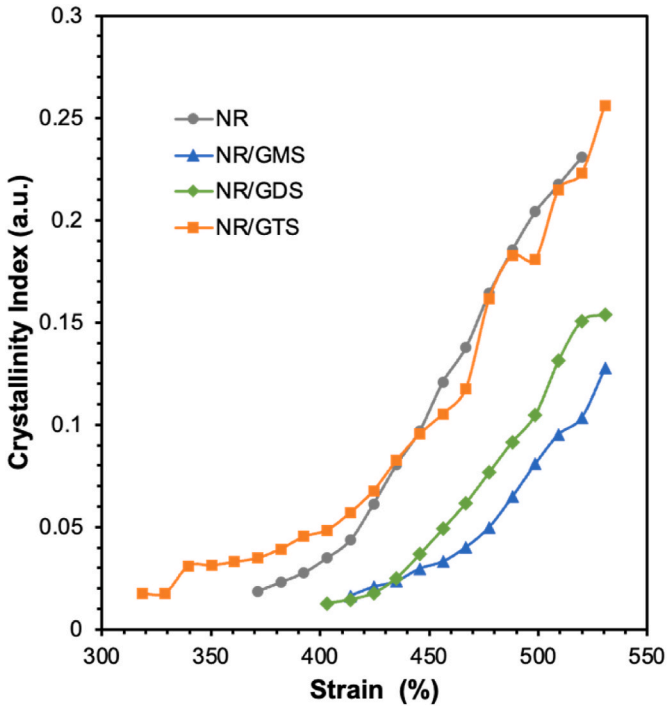

Fig. 5. Crystallinity index of NR, NR/GMS, NR/GDS, and NR/GTS as a function of strain. The displayed sample is the one whose SIC onset strain was closest to the average.

GDS and GTS, respectively. The 1D WAXD patterns for pure glycerol stearates were also measured (Fig. S3), and these peaks matched with that of the NR mixture. This result corresponds with the DSC result that NR and glycerol stearates are not compatible, and the crystalline domain of glycerol stearates are separated from the NR phase. From that perspective, the SIC promoting factor of GTS is considered to be heterogeneous nucleating effect [22], resulting from the affinity of the microcrystals to the highly hydrophobic NR matrix. While GDS and GMS, which contain hydroxyl groups, cannot contact NR chains and merely occupies space to reduce crosslink density, GTS, which lack hydroxyl groups and being highly hydrophobic, exhibits a higher affinity to the NR matrix and provide the surface energy that promotes the formation of crystal nuclei. At first sight, the good affinity of GTS to NR derived from its high hydrophobicity seem contradictory to its phase separation as crystals within the rubber matrix. However, this can be explained by the exceptionally strong packing of the alkyl chains, which gives GTS extremely high crystalline, making such behavior feasible. Indeed, glycerol trioleate, which has unsaturated alkyl chains and exists as oil at room temperature, is incorporated into rubber matrix to work as plasticizer, which has opposite effect to enhance SIC behavior [23].

3.4. Similarity between strain-induced crystallization behavior and thermal-induced crystallization

To evaluate the process of SIC, crystallinity was calculated for each sample of NR, NR/GMS, NR/GDS, and NR/GTS. The calculation process is shown in Fig. S4. Fig. 5 shows the stress-crystallinity index curves for NR, NR/GMS, NR/GDS and NR/GTS. For all samples, the crystallinities increase as the stress become larger. The theoretical onset strain of SIC can be understood as the point where the extrapolated crystallinity curve is predicted to reach zero, and the onset strain determined in previous section are likely to correspond to that. It is worth noting that there is a plateau region between the initial crystallization and subsequent crystal growth in NR/GTS, whose SIC onset showed lowest strain, whereas the crystal growth occurs soon after the crystallization in the other samples. This supports that GTS exhibits nucleating agent effect, and that the presence of GTS microcrystals decreases the nucleation energy required for NR crystal nucleation, resulting in an earlier SIC response as the intrinsic onset strain of SIC is reached.

Furthermore, since the degree of crystallinity of NR/GTS stabilizes to the same levels with NR at high strain region, this curve can be interpreted as the boundary of maximum crystallinity. With GTS microcrystal, the crystallinity follows the maximum level against strain. On the other hand, in pure NR, "superstretching" occurs beyond the intrinsic onset strain of SIC, and crystal nucleation and growth take place almost simultaneously once a certain strain threshold is reached. The role of GTS microcrystals is to prevent this "superstretching," and immediately inducing the crystallization at intrinsic onset strain of SIC, by providing surfaces or sites that lower the energy barrier for crystal nucleation.

This phenomenon can be compared to supercooling observed when a material transitions from a liquid to a solid state upon temperature reduction. Supercooling occurs when a liquid is cooled below its freezing point without undergoing a phase transition into a solid. In this

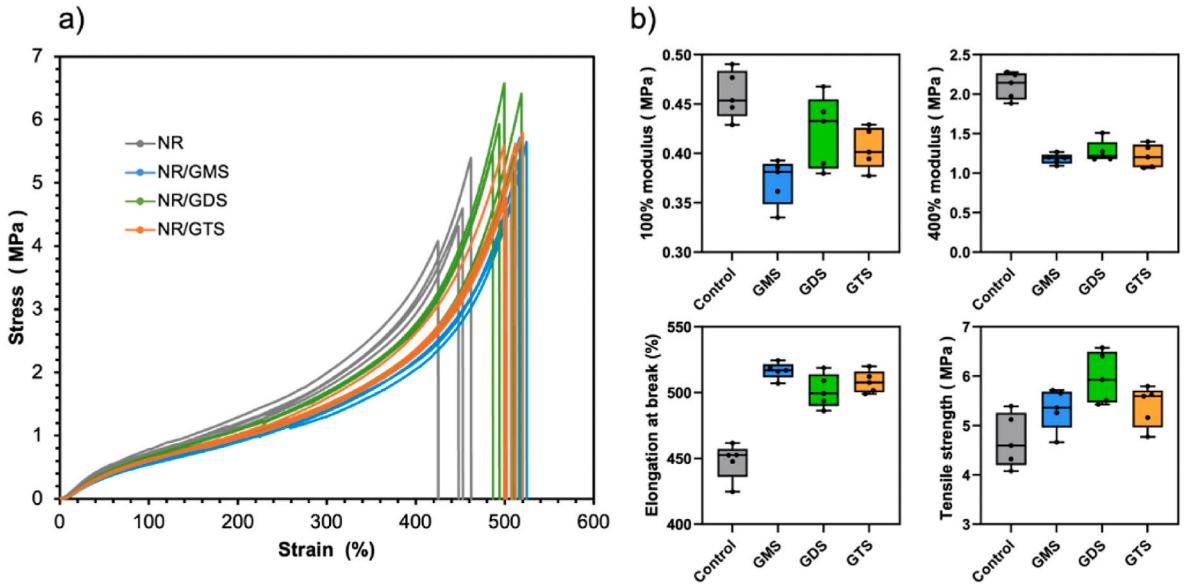

Fig. 6. Comparison of a) stress-strain curves and b) mechanical properties for NR, NR/GMS, NR/GDS, and NR/GTS. ($n = 5$).

state, the liquid remains in a metastable state because crystal nucleation, which is necessary for solidification, does not occur. This phenomenon happens because the system lacks the necessary nucleation energy. As a result, the liquid can reach temperatures significantly below its freezing point before crystallization occurs. However, when impurities are introduced into the system, they can act as nucleating agents, providing surfaces or sites that lower the energy barrier for crystal nucleation. These impurities facilitate the organization of molecules into a crystalline structure by serving as a template or seed for nucleation. This reduces the degree of supercooling and allows solidification to occur immediately upon reaching the freezing point. When the supercooling is substituted to SIC behavior, increasing strain in NR is assigned to lowering the temperature of a material. The pure NR experiences "superstretching" beyond the intrinsic onset strain of SIC before a sudden increase in crystallinity. On the other hand, with GTS, SIC occurs at the intrinsic onset strain of SIC immediately, consistently following the boundary of maximum crystallinity.

3.5. Tensile properties of NR, NR/GMS, NR/GDS and NR/GTS

The stress-strain curves were obtained as the result of uniaxial single-mode tensile test (Fig. 6a). It was commonly observed for all samples that the slope of the curve remained relatively small in the low-strain region, while the notable increase in slope was observed in the high-strain region. Generally, this stress upturn is attributed to the synergistic effect of the SIC onset and the achievement of maximum molecular chain extension [24]. The results showed no significant differences among NR/GMS, NR/GDS, and NR/GTS, and the addition of glycerol stearates resulted in a shift of the stress upturn point toward larger strain levels regardless of the type of the lipids. This shift is especially reflected in the decrease of modulus at 400 % strain and the corresponding increase of elongation at break, while no significant difference was recognized in tensile strength. (Fig. 6b). Such changes are considered to be attributed to the depression of the crosslink density mentioned above. Theoretically, the elastic modulus is proportional to the crosslink density, and the elongation at break decreases as the crosslink density increases. The results obtained in this study are in clear agreement with this relationship; both the elongation at break and the elastic modulus correspond well to the relative levels of crosslink density. Therefore, it can be assumed that the dominant factor influencing the results of the tensile tests is the crosslink density, and that the effect of SIC promotion is negligible compared to that of crosslink density in this context since the order of the stress upturn in the curves does not correspond to that of the SIC.

3.6. The feasibility of naturally occurring network

The results of both the tensile test and the swelling test consistently indicate that the crosslink density decreased for all lipids, regardless of the presence of hydroxyl groups. This suggests that a naturally occurring network, via hydrogen bonding between hydroxyl groups and the terminal ends of rubber molecules, was not formed, and consequently, SIC was not promoted.

In this case, the primary reason why hydroxyl groups did not participate in interactions is that GMS and GDS, which contain hydroxyl groups, did not exhibit compatibility with the NR matrix. However, numerous previous studies have supported the interaction between functional groups of non-rubber components and the α-terminal of natural rubber [13,14], with many suggesting that lipids are generally compatible with NR and working as crosslinking point [7–9].

This discrepancy is likely due to differences in the mixing method. The results indicates that, in the organic solvent mixing system used in this study, it is unlikely that the hydrophilic region of lipids preferentially interacts with the terminal structure of NR chains after intruding into the abundant hydrophobic regions. For interactions between lipids and the α-terminal to occur, some inhomogeneous structure must be present that allows the hydrophilic regions to stably exist within the NR matrix [25,26]. However, such a structure is likely lost in solution mixing method employed here. In the rubber industry, additives are thoroughly blended during the compounding process using roll mills. Therefore, the findings in this study do not deny the potential contribution of naturally occurring network to the SIC behavior of NR.

4. Conclusion

It was confirmed that the addition of GMS, GDS, and GTS introduced changes in the SIC behavior and tensile properties of NR. As the results of the DSC and swelling test suggested, all the lipids existed as a crystalline domain in NR matrix, decreasing the crosslink density. However, the WAXD profiles showed that the addition of GTS promoted SIC onset, which is due to GTS microcrystals acting as nucleating agents, while the addition of GMS and GDS did not show the nucleating agent effect and delayed SIC onset. The unique nucleating agent effect of GTS comes from the combination of its strong affinity to the NR matrix phase, which is related to the high hydrophobicity, and the highly crystalline domain, which is attributed to the efficient packing of its alkyl chains. On the other hand, no significant interaction was observed between the hydroxyl group of GMS or GDS and the terminal structure of NR molecules to form naturally occurring network. Therefore, it is concluded that the dominant factor that promotes SIC in the solvent-mixed systems in this study is the nucleating agent effect derived from esterified fatty acids, rather than naturally occurring network derived from hydroxyl groups. Nevertheless, in terms of mechanical property evaluation, the effect of SIC behavior was negligible compared to the effect of crosslink density, making it difficult to assert that the addition of GTS, which promoted SIC, improved the tensile properties of NR. Our findings demonstrate that nucleation step is the rate-determining step in the SIC process, and this can be understood in analogy to supercooling and depression of the freezing point. This insight is highly significant for elucidating the mechanism of SIC occurrence and should be considered in future research.

CRediT authorship contribution statement

Tomoaki Nakatsuka: Writing – original draft, Visualization, Methodology, Investigation, Formal analysis, Data curation, Conceptualization. **Hiroyasu Masunaga:** Methodology, Formal analysis, Data curation. **Yui Tsuji:** Methodology, Investigation. **Keiji Numata:** Writing – review & editing, Supervision, Project administration, Funding acquisition, Conceptualization.

Declaration of competing interest

The authors declare that the research was conducted in the absence of any commercial or financial relationships that could be construed as potential conflicts of interest.

Acknowledgement

This work was supported by Japan Science and Technology Agency CREST (Grant Number JPMJCR2091), JST COI-Next (Grant Number JPMJPF2114), and the MEXT Program: Data Creation and Utilization-Type Material Research and Development Project (Grant Number JPMXP1122714694), Japan. The X-ray experiments were performed at BL05XU of SPring-8 (Harima, Japan). Sincere appreciation is extended to Bridgestone Corporation for kindly providing the natural rubber samples.

Appendix A. Supplementary data

Supplementary data to this article can be found online at https://doi.org/10.1016/j.polymer.2025.128575.

Data availability

Data will be made available on request.

References

[1] Y. Ikeda, Y. Yasuda, S. Makino, S. Yamamoto, M. Tosaka, K. Senoo, S. Kohjiya, Strain-induced crystallization of peroxide-crosslinked natural rubber, Polymer 48 (5) (2007) 1171–1175.

[2] M. Tosaka, S. Murakami, S. Poompradub, S. Kohjiya, Y. Ikeda, S. Toki, I. Sics, B. S. Hsiao, Orientation and crystallization of natural rubber network as revealed by WAXD using synchrotron radiation, Macromolecules 37 (9) (2004) 3299–3309.

[3] N. Candau, L. Chazeau, J.M. Chenal, C. Gauthier, E. Munch, A comparison of the abilities of natural rubber (NR) and synthetic polyisoprene cis-1,4 rubber (IR) to crystallize under strain at high strain rates, Phys. Chem. Chem. Phys. 18 (5) (2016) 3472–3481.

[4] Y. Kitamura, K. Okada, H. Masunaga, M. Hikosaka, Role of strain rate in the strain-induced crystallization (SIC) of natural and synthetic isoprene rubber, Polym. J. 51 (2) (2018) 221–226.

[5] Y. Tanaka, Structural characterization of natural polyisoprenes: solve the mystery of natural rubber based on structural study, Rubber Chem. Technol. 74 (3) (2000) 355–375.

[6] X. Qi, D. Yue, Effect of stereoregularity on strain-induced crystallization and mechanical properties of natural rubber, Macromolecules 57 (9) (2024) 4045–4053.

[7] C.-C. Wang, H.-B. Yin, S.-J. Bai, R. Zhang, C.-H. Li, M.-Z. Tang, Y.-X. Xu, Probe the terminal interactions and their synergistic effects on polyisoprene properties by mimicking the structure of natural rubber, Polymer 237 (2021).

[8] Y. Wang, H. Liu, H. Yu, P. Zhao, Q. Wang, L. Liao, M. Luo, T. Zheng, S. Liao, Z. Peng, New insight into naturally occurring network and entanglements induced strain behavior of vulcanized natural rubber, Polymer 241 (2022).

[9] J. Wu, W. Qu, G. Huang, S. Wang, C. Huang, H. Liu, Super-resolution fluorescence imaging of spatial organization of proteins and lipids in natural rubber, Biomacromolecules 18 (6) (2017) 1705–1712.

[10] L. Tarachiwin, J. Sakdapipanich, K. Ute, T. Kitayama, T. Bamba, E. Fukusaki, A. Kobayashi, Y. Tanaka, Structural characterization of α-Terminal group of natural rubber. 1. Decomposition of branch-points by lipase and phosphatase treatments, Biomacromolecules 6 (4) (2005) 1851–1857.

[11] T. Kitaura, M. Kobayashi, L. Tarachiwin, H. Kum-ourm, A. Matsuura, K. Fushihara, K. Ute, Characterization of natural rubber end groups using high-sensitivity NMR, Macromol. Chem. Phys. 219 (3) (2018).

[12] M. Oouchi, J. Ukawa, Y. Ishii, H. Maeda, Structural analysis of the terminal groups in commercial hevea natural rubber by 2D-NMR with DOSY filters and Multiple-WET methods using ultrahigh-field NMR, Biomacromolecules 20 (3) (2019) 1394–1400.

[13] M. Dixit, T. Taniguchi, Role of terminal groups of cis-1,4-Polyisoprene chains in the formation of physical junction points in natural rubber, Biomacromolecules 24 (8) (2023) 3589–3602.

[14] J. Gimenez-Dejoz, K. Tsunoda, Y. Fukushima, K. Numata, Computational study of the interaction between natural rubber α-terminal groups and l-quebrachitol, one of the major components of natural rubber, Polym. J. 54 (2) (2021) 229–233.

[15] S. Kawahara, K. Takano, J. Yunyongwattanakorn, Y. Isono, M. Hikosaka, J. T. Sakdapipanich, Y. Tanaka, Crystal nucleation and growth of natural rubber purified by deproteinization and trans-esterification, Polym. J. 36 (5) (2004) 361–367.

[16] Y. Zhou, K. Kosugi, Y. Yamamoto, S. Kawahara, Effect of non-rubber components on the mechanical properties of natural rubber, Polym. Adv. Technol. 28 (2) (2017) 159–165.

[17] P.J. Flory, J. Rehner, Statistical mechanics of cross-linked polymer networks II. Swelling, J. Chem. Phys. 11 (11) (1943) 521–526.

[18] Y. Wang, L. Liao, R. Wang, H. Yu, T. Zheng, Y. Lian, M. Luo, S. Liao, H. Liu, Z. Peng, Research of strain induced crystallization and tensile properties of vulcanized natural rubber based on crosslink densities, Ind. Crop. Prod. 202 (2023).

[19] V. Rao, J. Johns, Thermal behavior of chitosan/natural rubber latex blends TG and DSC analysis, J. Therm. Anal. Calorim. 92 (3) (2008) 801–806.

[20] P.S. Thomas, A.A. Abdullateef, M.A. Al-Harthi, A.A. Basfar, S. Bandyopadhyay, M. A. Atieh, S.K. De, Effect of phenol functionalization of carbon nanotubes on properties of natural rubber nanocomposites, J. Appl. Polym. Sci. 124 (3) (2011) 2370–2376.

[21] P. Kumari, G. Unnikrishnan, Thermal properties of compatibilized and filled natural rubber/acrylonitrile butadiene rubber blends, J. Therm. Anal. Calorim. 114 (1) (2013) 67–75.

[22] F.L. Binsbergen, Heterogeneous nucleation in the crystallization of polyolefins: part 1. Chemmical and physical nature of nucleating agents, Polymer 11 (5) (1970) 253–267.

[23] M. Jarnthong, N. Lopattananon, Y. Li, H. Yu, R. Wang, Y. Wang, H. Liu, L. Liao, Z. Peng, Performance of moringa oil as an effective bioplasticizer on static and dynamic mechanical properties of natural rubber vulcanizates, ACS Sustain. Chem. Eng. 12 (16) (2024) 6440–6450.

[24] S. Toki, J. Che, L. Rong, B.S. Hsiao, S. Amnuaypornsri, A. Nimpaiboon, J. Sakdapipanich, Entanglements and networks to strain-induced crystallization and stress–strain relations in natural rubber and synthetic polyisoprene at various temperatures, Macromolecules 46 (13) (2013) 5238–5248.

[25] S. Kumarn, N. Churinthorn, A. Nimpaiboon, M. Sriring, C.C. Ho, A. Takahara, J. Sakdapipanich, Investigating the mechanistic and structural role of lipid hydrolysis in the stabilization of ammonia-preserved hevea rubber latex, Langmuir 34 (43) (2018) 12730–12738.

[26] M. Sriring, A. Nimpaiboon, S. Kumarn, K. Higaki, Y. Higaki, K. Kojio, A. Takahara, C.C. Ho, J. Sakdapipanich, Film formation process of natural rubber latex particles: roles of the particle size and distribution of non-rubber species on film microstructure, Colloids Surf. A Physicochem. Eng. Asp. 592 (2020).